Swift-Hohenberg equation with broken reflection symmetry

J. Burke,[1,*] S. M. Houghton,[2,†] and E. Knobloch[3,‡]

[1]*Center for BioDynamics, Boston University, Boston, MA 02215, USA*

[2]*School of Mathematics, University of Leeds, LS2 9JT, UK.*

[3]*Department of Physics, University of California, Berkeley, CA 94720, USA.*

(Dated: July 28, 2009)

Abstract

The bistable Swift-Hohenberg equation possesses a variety of time-independent spatially localized solutions organized in the so-called snakes-and-ladders structure. This structure is a consequence of a phenomenon known as homoclinic snaking, and is in turn a consequence of spatial reversibility of the equation. We examine here the consequences of breaking spatial reversibility on the snakes-and-ladders structure. We find that the localized states now drift, and show that the snakes-and-ladders structure breaks up into a stack of isolas. We explore the evolution of this new structure with increasing reversibility breaking and study the dynamics of the system outside of the snaking region using a combination of numerical and analytical techniques.

PACS numbers: 47.54.-r, 47.20.Ky

Keywords: Swift-Hohenberg equation; Symmetry breaking

*Electronic address: jb@math.bu.edu

†Electronic address: smh@maths.leeds.ac.uk

‡Electronic address: knobloch@berkeley.edu

I. INTRODUCTION

The so-called 23 Swift-Hohenberg equation takes the form

$$\partial_t u = ru - \left(1+\partial_x^2\right)^2 u + b_2 u^2 - u^3 \tag{1}$$

and admits multiple stationary spatially localized states on the real line within the so-called snaking or pinning region [1, 2]. These are organized in a structure that has been called the snakes-and-ladders structure, shown in Fig. 1. The snaking or pinning region $r_{P1} < r < r_{P2}$ is defined by the asymptotic location of the saddle-nodes high up the snaking structure. The point $r = r_M$ corresponds to the Maxwell point for this system, determined by the twin conditions $F = H = 0$ [2, 3]. At this point the energy $F[u_p(x)]$ of the spatially periodic state $u_p(x)$ with wavelength λ_M is equal to the energy $F[0] = 0$ of the trivial state $u = 0$, where

$$F[u(x)] = \int_{-\infty}^{\infty} \mathrm{d}x \left\{ -\frac{1}{2} r u^2 + \frac{1}{2}\left[(1+\partial_x^2)u\right]^2 - \frac{1}{3} b_2 u^3 + \frac{1}{4} u^4 \right\}. \tag{2}$$

The wavelength $\lambda(r)$ of the localized states high up the snaking structure is determined from the requirement that any steady state asymptotic to $u = 0$ as $|x| \to \infty$ must lie in the hypersurface $H = 0$ containing $u = 0$, where

$$H \equiv -\frac{1}{2}(r-1)\, u^2 + [\partial_x u]^2 - \frac{1}{2}[\partial_x^2 u]^2 + \partial_x u \partial_x^3 u - \frac{1}{3} b_2 u^3 + \frac{1}{4} u^4 \tag{3}$$

is the Hamiltonian conserved by the time-independent version of Eq. (1) written as a dynamical system in space. These two conditions together determine both $r = r_M$ and $\lambda(r_M) \equiv \lambda_M$.

The structure summarized in Fig. 1 may be thought of as the result of broadening of the classical Maxwell point between a pair of homogeneous equilibria in a variational system due to the pinning of the fronts bounding the localized state to the periodic structure within [1, 2, 4, 5]. Mathematically, it is a consequence of spatial reversibility, i.e., the invariance of Eq. (1) under

$$R: \quad x \to -x, \quad u \to u, \tag{4}$$

as discussed in Refs. [5, 6, 7, 8]. It is therefore of interest to examine the consequence of weak breaking of the symmetry (4). In this paper we examine the effect of adding a dispersive term to Eq. (1), and study the equation

$$\partial_t u = ru - \left(1+\partial_x^2\right)^2 u + \gamma \partial_x^3 u + b_2 u^2 - u^3 \tag{5}$$

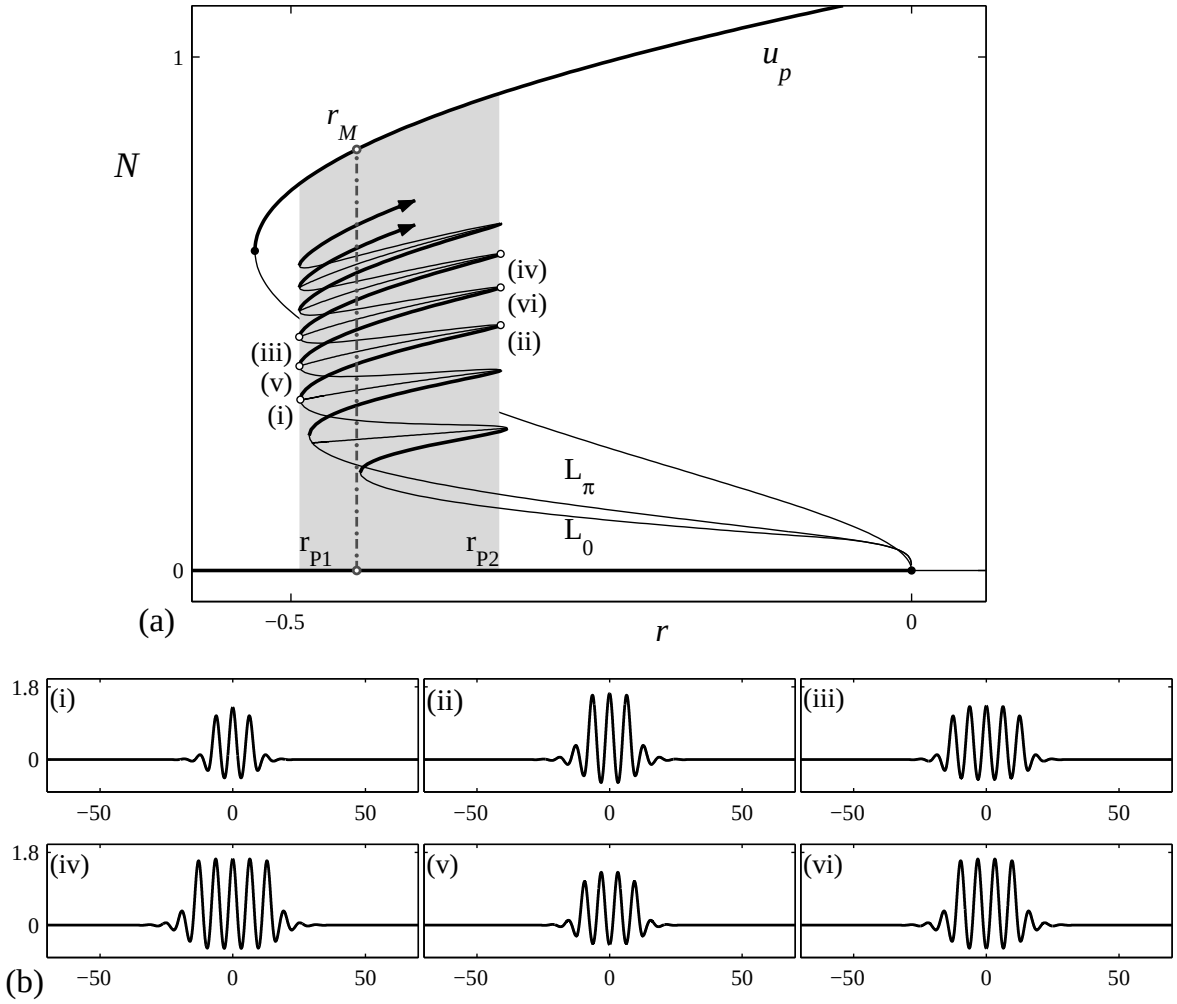

FIG. 1: (a) Homoclinic snaking in Eq. (1) when $b_2 = 2$. Stable (unstable) states are indicated by thick (thin) lines. N is the L^2 norm per unit length. (b) Sample localized profiles $u(x)$. States (i)-(iv) are located at successive saddle-nodes on the L_0 branch; (v)-(vi) lie on L_π.

for $b_2 = 2$ and small values of the coefficient γ.

II. NUMERICAL RESULTS

Steadily drifting localized states can be obtained as solutions of the time-independent ordinary differential equation

$$ru - \left(1 + \partial_\xi^2\right)^2 u + v\partial_\xi u + \gamma\partial_\xi^3 u + b_2 u^2 - u^3 = 0, \tag{6}$$

subject to $u \to 0$ as $|\xi| \to \infty$. Here $\xi \equiv x - vt$ and the drift speed v is computed as part of the solution, i.e., it is a (nonlinear) eigenvalue.

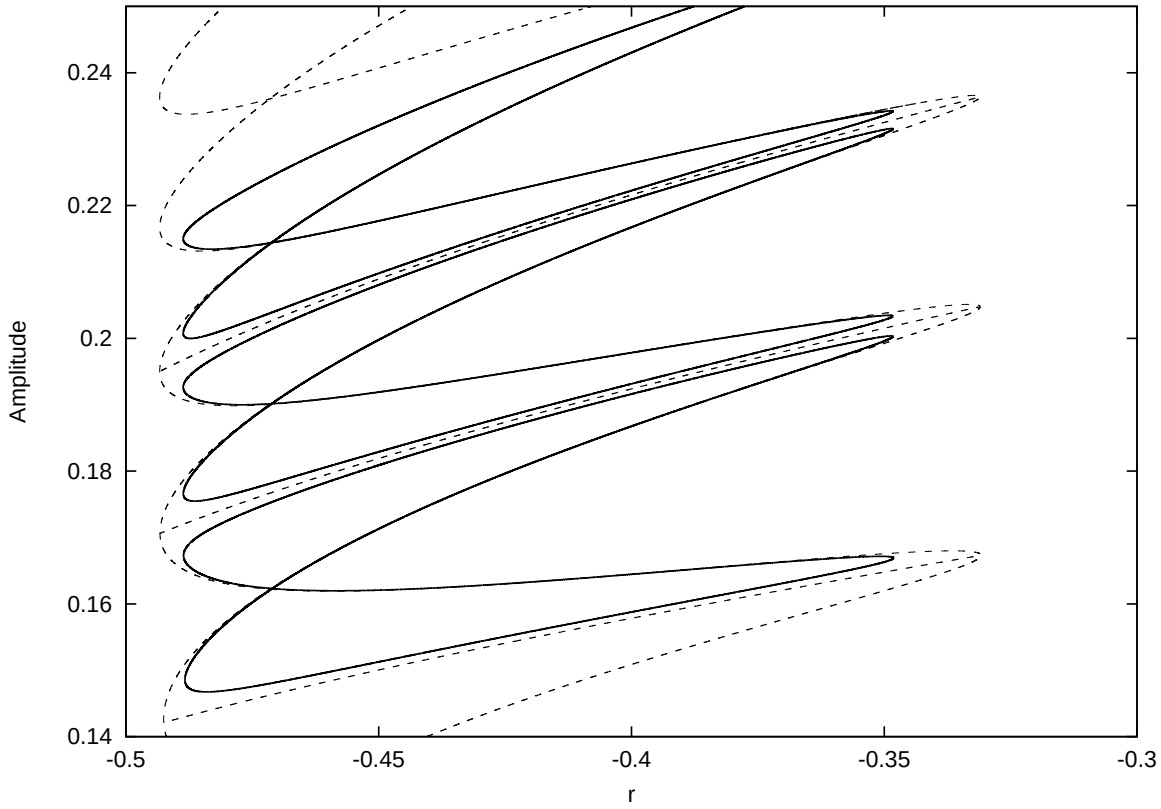

FIG. 2: The breakup of the snakes-and-ladders structure into a stack of isolas when $\gamma = 0.05$ (solid line). The underlying snakes-and-ladders structure ($\gamma = 0$) is shown for comparison (dashed line). Parameter: $b_2 = 2$.

The loss of reversibility symmetry destroys the pitchfork bifurcations responsible for the rung states present near each saddle-node, resulting in a stack of isolas as shown in Fig. 2. The drift speed of the pattern at onset ($r = 0$) is given by $v = \gamma$, and remains of order γ for larger amplitudes (Fig. 3). Figure 4 shows that the isolas gradually shrink towards $r = r_{M1}$ as γ increases, and disappear completely near $\gamma = 0.4$ (for $b_2 = 2$). Throughout this process the drift speed remains $O(\gamma)$ as shown in Fig. 5.

Different cuts through parameter space result in different morphologies. With $\gamma = 0.4 + r$ the sign of the dispersive term changes across the pinning region resulting in a pair of intertwined snakes instead of a stack of isolas (Fig. 6).

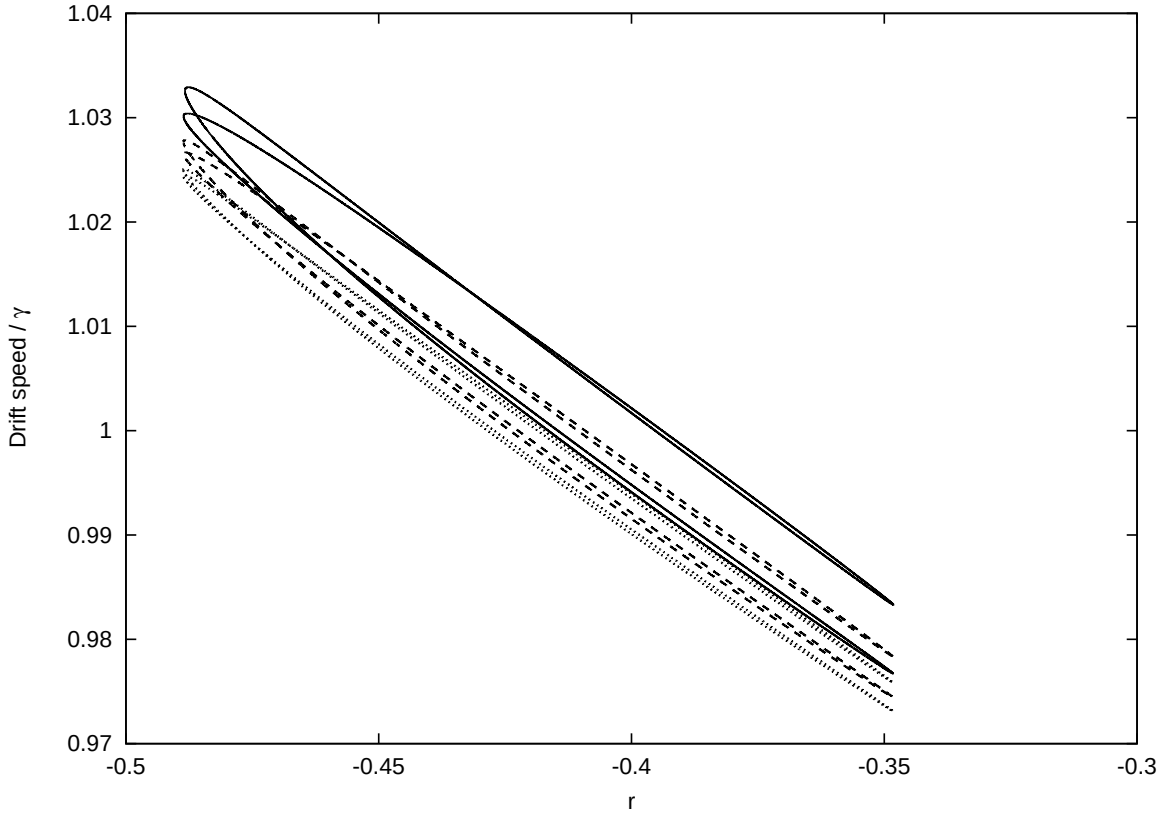

FIG. 3: Drift speeds (normalised against γ) along the three isolas shown in Fig. 2. The drift speed decreases with increasing width (solid to dashed to dotted) of the localized state. Parameter: $b_2 = 2$.

III. DEPINNING

We now examine the dynamics outside of the pinning region. When $\gamma = 0$ and $r > r_{P2}$ the fronts bounding the localized state unpin, and since the periodic state has lower energy than $u = 0$ the fronts move apart allowing the periodic state to invade the entire domain. The opposite occurs when $r < r_{P1}$ and the fronts move so as to eliminate the localized structure. The growth/decay of the localized state takes place via successive nucleation/destruction of structures at either front region. When $\gamma = 0$ these processes take place symmetrically, maintaining the overall reflection symmetry of the localized state as it grows or decays. Figures 7(a) and 7(b) show that this is no longer the case when $\gamma \neq 0$: for small $\delta \equiv r - r_{P2}$ (long nucleation time) the localized state grows only at the leading front while for larger δ it grows at both ends, albeit asymmetrically. However, at yet larger values of γ nucleation

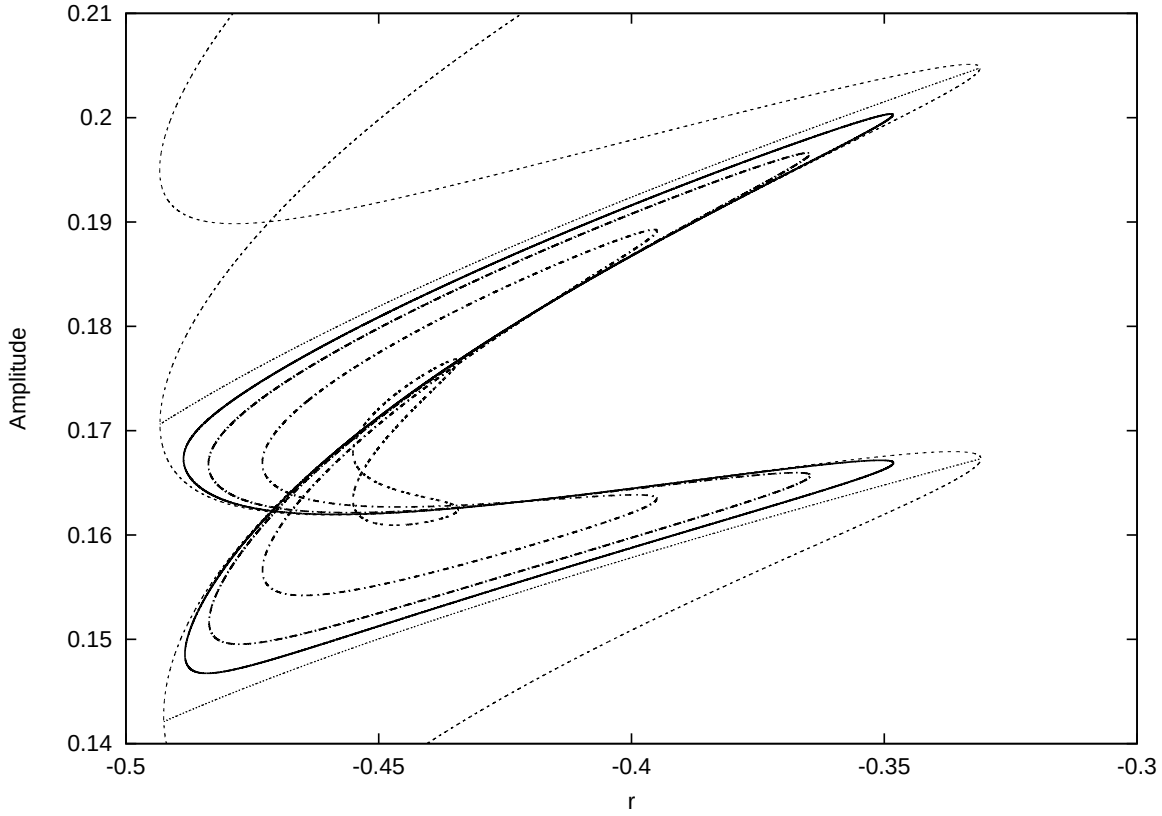

FIG. 4: Isolas formed within a pair of rungs of the snakes-and-ladders structure when $\gamma = 0.05, 0.10, 0.20$ and 0.35. The underlying snakes-and-ladders structure is indicated by a short-dashed line. As γ increases the size of the isola decreases. Parameter: $b_2 = 2$.

is again restricted to the leading front (Fig. 7(c)).

IV. ANALYSIS

The time to nucleate a new wavelength can be computed by projecting the dynamics near the boundary of the pinning region onto the neutral modes of the localized structure present at $r = r_{P1}$ or $r = r_{P2}$ [2, 9]. This procedure can be extended to the case $\gamma \neq 0$, as we now show.

We anticipate that when $\gamma \neq 0$ all patterns will drift; this drift is a consequence of the excitation of the translation mode U_0' and takes place on the timescale γ^{-1}. We set $r = r_{P2} + \delta$, $|\delta| \ll 1$, and write

$$u(x,t) = u_0(x + \theta(T)) + |\delta|^{1/2} u_1(x + \theta(T), \tau) + |\delta| u_2(x + \theta(T), \tau) + \ldots, \qquad (7)$$

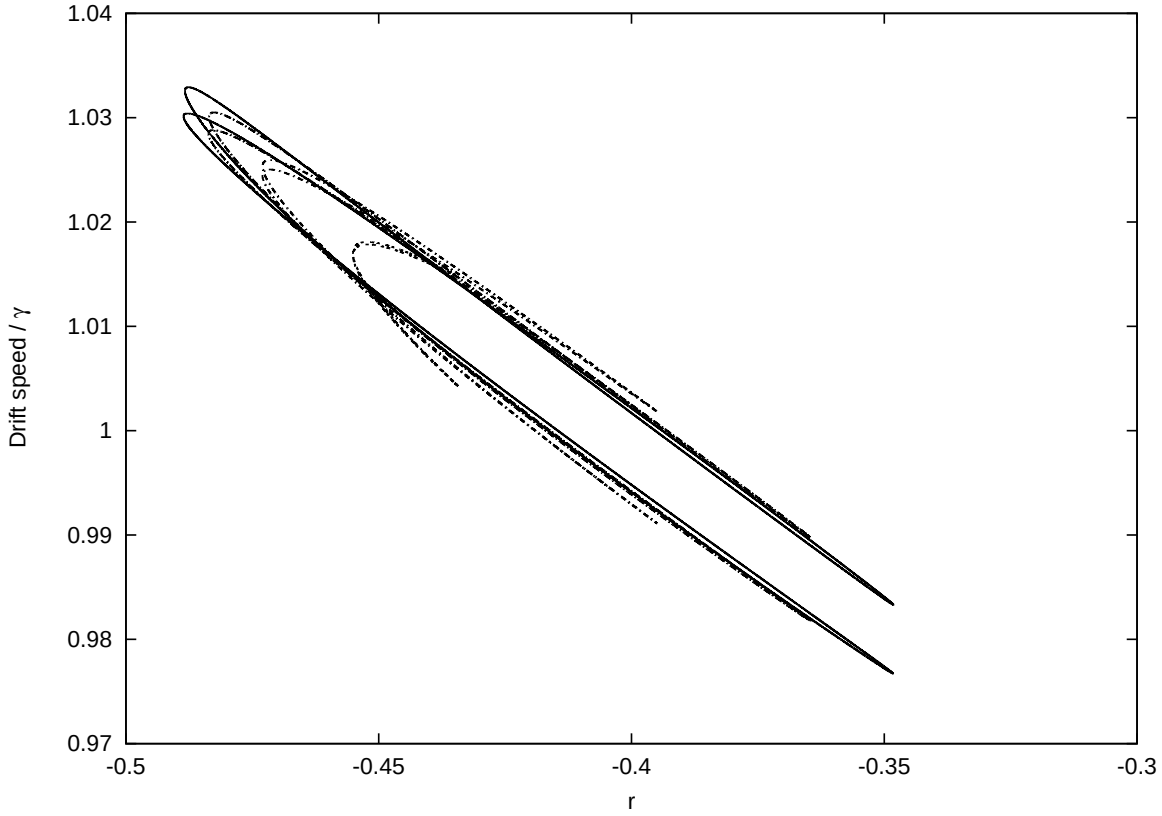

FIG. 5: Drift speeds along the isolas in Fig. 4, as indicated by the corresponding line type.

where $\theta(T)$ is the spatial phase of the pattern, $\tau = |\delta|^{1/2}t$ and $T = |\delta|t$. Finally, we take $\gamma = \sigma|\delta|$, $\sigma = O(1)$, to include γ in the expansion at the correct order.

The leading order problem is given by

$$r_{P2}u_0 - \left(1 + \partial_x^2\right)^2 u_0 + b_2 u_0^2 - u_0^3 = 0, \tag{8}$$

with solution $u_0 = U_0(x + \theta(T))$. In the following we pick the solution at the fourth saddle-node on branch L_0 (Fig. 8) for all explicit computations.

At order $O(|\delta|^{1/2})$ we obtain

$$\mathcal{L}u_1 = 0, \tag{9}$$

where $\mathcal{L} \equiv r_{P2} - (1 + \partial_x^2)^2 + 2b_2U_0 - 3U_0^2$ and is self-adjoint. At a saddle-node high up the snaking branches $\mathcal{L}$ possesses two null eigenfunctions, a symmetric mode $\tilde{u}_{10}$ and the antisymmetric translation mode $\tilde{u}_{12} \equiv U_0'$. In addition, there is a third nearly neutral antisymmetric mode, $\tilde{u}_{11}$, responsible for the branching of asymmetric states exponentially close to each saddle-node (Fig. 1). These eigenfunctions are also shown in Fig. 8. Since the

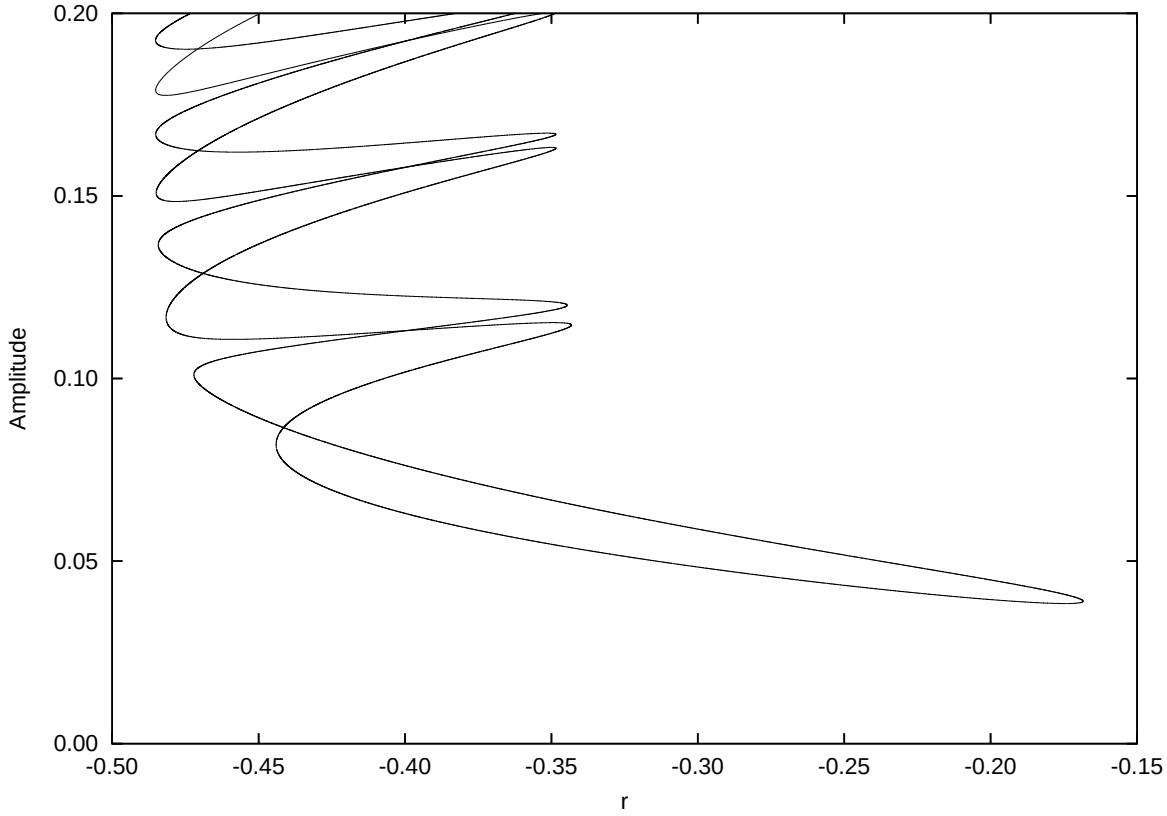

FIG. 6: Reconnection of the snakes-and-ladders structure when $\gamma = 0.4 + r$. Parameter: $b_2 = 2$.

translation mode is already included in the phase θ we have

$$u_1 = a(\tau)\tilde{u}_{10}(x + \theta(T)) + b(\tau)\tilde{u}_{11}(x + \theta(T)), \tag{10}$$

where $a(\tau)$, $b(\tau)$ and $\theta(T)$ are to be determined.

At order $O(|\delta|)$ we obtain

$$U_0'\theta_T + u_{1\tau} = \mathcal{L}u_2 + \mathrm{sgn}(\delta)U_0 + \sigma U_0''' + (b_2 - 3U_0)\, u_1^2. \tag{11}$$

Solvability conditions for u_2 follow on multiplying Eq. (11) in turn by $\tilde{u}_{10}$, $\tilde{u}_{11}$ and U_0', and integrating over the real line. For the profile in Fig. 8 the U_0' solvability condition yields, to leading order,

$$\theta_T = -0.9663\sigma. \tag{12}$$

Thus the drift speed, $\theta_t = -0.9663\gamma$ in unscaled variables, increases (at leading order) linearly with γ. The resulting prediction for $\gamma = 0.001$ agrees very well with the measured speed 0.0009589. Measurements show that the drift speed is almost independent of δ, i.e.,

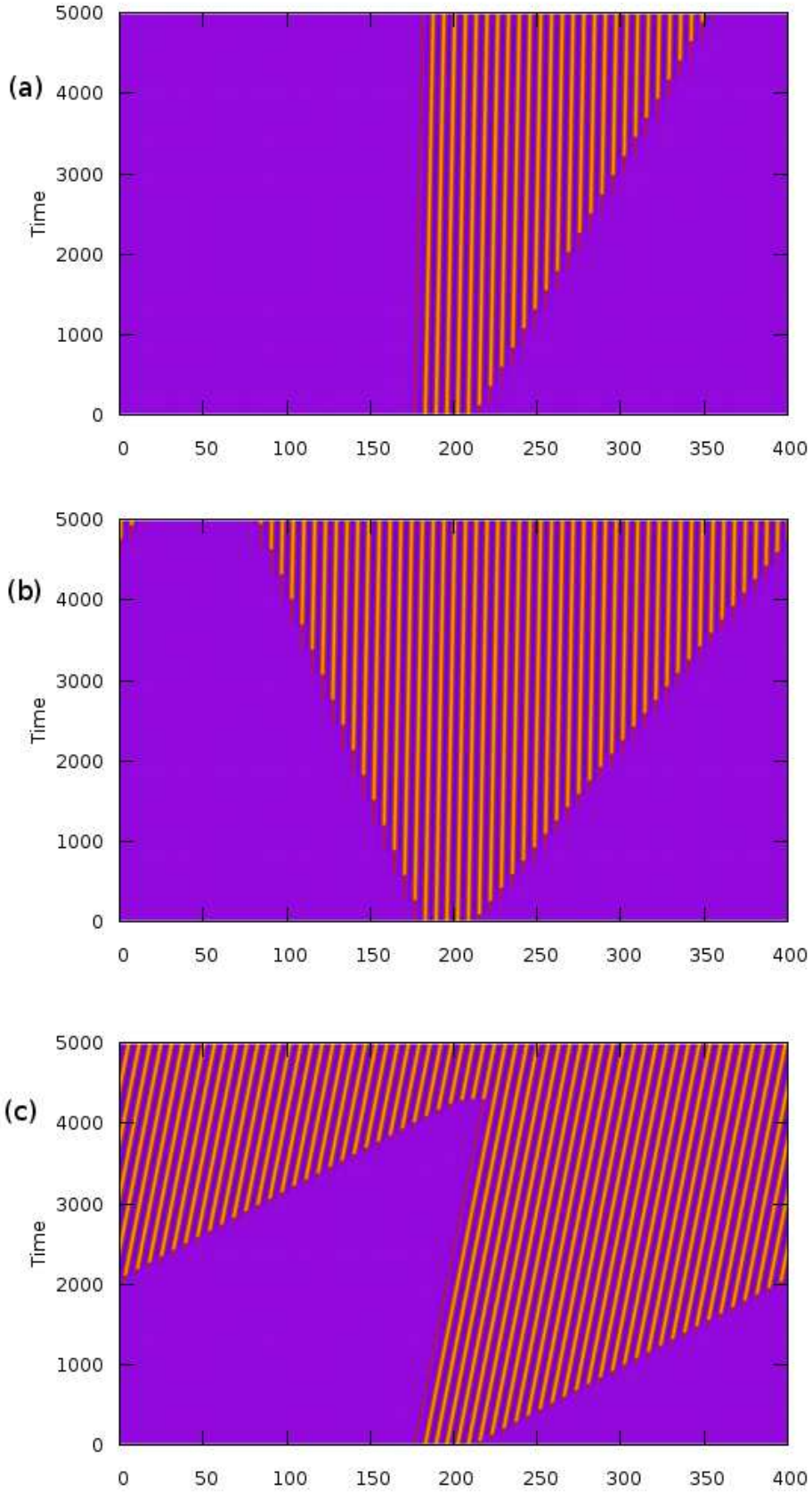

FIG. 7: Space-time evolution of solutions of Eq. (5). (a) $\gamma = 0.001$ and $r = r_{P2} + 0.00015$: the patterned region grows at the leading front only. (b) $\gamma = 0.001$ and $r = r_{P2} + 0.00065$: the patterned region grows on both ends, but at different rates. (c) $\gamma = 0.01$ and $r = r_{P2} + 0.00065$: nucleation again occurs at the leading front only. Parameter $b_2 = 2$ throughout.

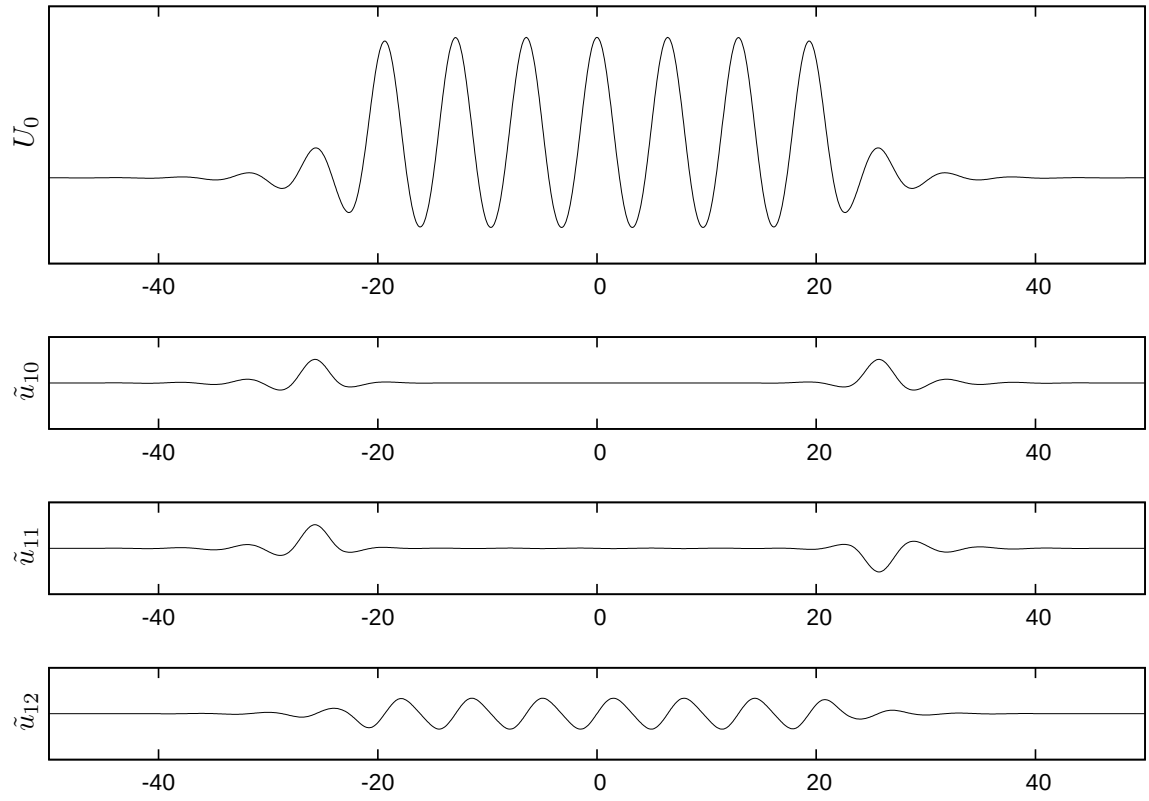

FIG. 8: Steady solution U_0 at the fourth saddle-node on the L_0 branch ($r = -0.33101564$). Lower panels show the three neutral eigenfunctions.

at leading order the drift speed is not related to the asymmetry of the pattern. On the other hand in writing Eq. (12) we have dropped two terms with $O(10^{-5})$ coefficients. These terms involve the overlap of $\tilde{u}_{12} \equiv U_0'$ and $\tilde{u}_{11}$ but these peak at different locations and their product is already small (Fig. 8). As a result two very small terms reflecting the effect of asymmetric nucleation of new cells fore and aft on the drift speed has been omitted.

The remaining solvability conditions yield the coupled equations

$$a_\tau = \alpha_1 \mathrm{sgn}(\delta) + \alpha_2 a^2 + \alpha_3 b^2 \tag{13}$$

$$b_\tau = -\beta\sigma + 2\alpha_4 ab. \tag{14}$$

The coefficients in this equation depend on the length $2L$ of the localized state. High up the snaking structure, $2L$ is large and the eigenfunctions $\tilde{u}_{10}$, $\tilde{u}_{10}$ consist, up to exponentially small terms, of pairs of nonoverlapping neutral modes localized at the bounding fronts [1, 8]. Consequently we may write $\tilde{u}_{10} = v(x+L)+v(x-L)$, $\tilde{u}_{11} = v(x+L)-v(x-L)$ for a suitable function $v(x)$, cf. Fig. 8. It follows that, up to exponentially small terms, $\alpha_2 = \alpha_3 = \alpha_4$. This

expectation is confirmed by a computation of the required integrals using the numerically generated profile U_0 in Fig. 8, together with the corresponding eigenfunctions. We obtain $\alpha_1 = 0.8411$, $\alpha_2 = \alpha_3 = \alpha_4 = 0.3904$ and $\beta = 0.2980$. These results are independent of which saddle-node is selected for the numerical evaluation provided the corresponding profile is sufficiently long that the instabilities at the front and back of the structure interact only exponentially weakly.

We now take linear combinations of the above equations,

$$(a \pm b)_\tau = \alpha_1 \mathrm{sgn}(\delta) \mp \beta\sigma + \alpha_2 (a \pm b)^2 , \tag{15}$$

and define the nucleation time at the leading front as the time [1]

$$T_{leading} \equiv \int_{-\infty}^{\infty} \frac{\mathrm{d}\tau}{a-b} = \frac{\pi}{\alpha_2^{1/2} (\alpha_1 \delta + \beta\gamma)^{1/2}}. \tag{16}$$

This time diverges (i.e., nucleation ceases) when $\delta_c^{leading} = -\beta\gamma/\alpha_1 = -0.3543\gamma$. The nucleation time at the trailing front is computed similarly, using $a+b$ instead of $a-b$ (see Fig. 8), and yields $\delta_c^{trailing} = 0.3543\gamma$. Thus the distance between the saddle-node of the drifting localized state and the boundary of the pinning region, $|r_{SN} - r_{P2}|$, is predicted to be 0.0003543 when $\gamma = 0.001$, a result consistent with the value 0.000356 obtained by numerical continuation. Moreover, the predicted leading and trailing nucleation times away from the saddle-node are also in excellent agreement with the results of direct numerical simulation (Fig. 9).

Observe that when $\sigma = 0$ (no dispersion), the amplitude $b = 0$ and Eqs. (13)-(14) reduce to those in [1]. Thus the asymmetry in the nucleation process is the result of excitation of the antisymmetric mode $\tilde{u}_{11}$ whenever $\sigma \neq 0$, and not of the translation mode.

V. DISCUSSION AND CONCLUSIONS

We have described the effects of weak breaking of the reversibility required for the presence of a snaking or pinning region in bistable systems with competing homogeneous and spatially periodic steady states, and the associated snakes-and-ladders structure. We have shown that for weak dispersion this structure breaks up into a stack of isolas of slowly drifting localized states and that these isolas shrink and eventually vanish as dispersion increases. Stacks of isolas are characteristic of multipulse homoclinic orbits as well [10, 11]. We have also

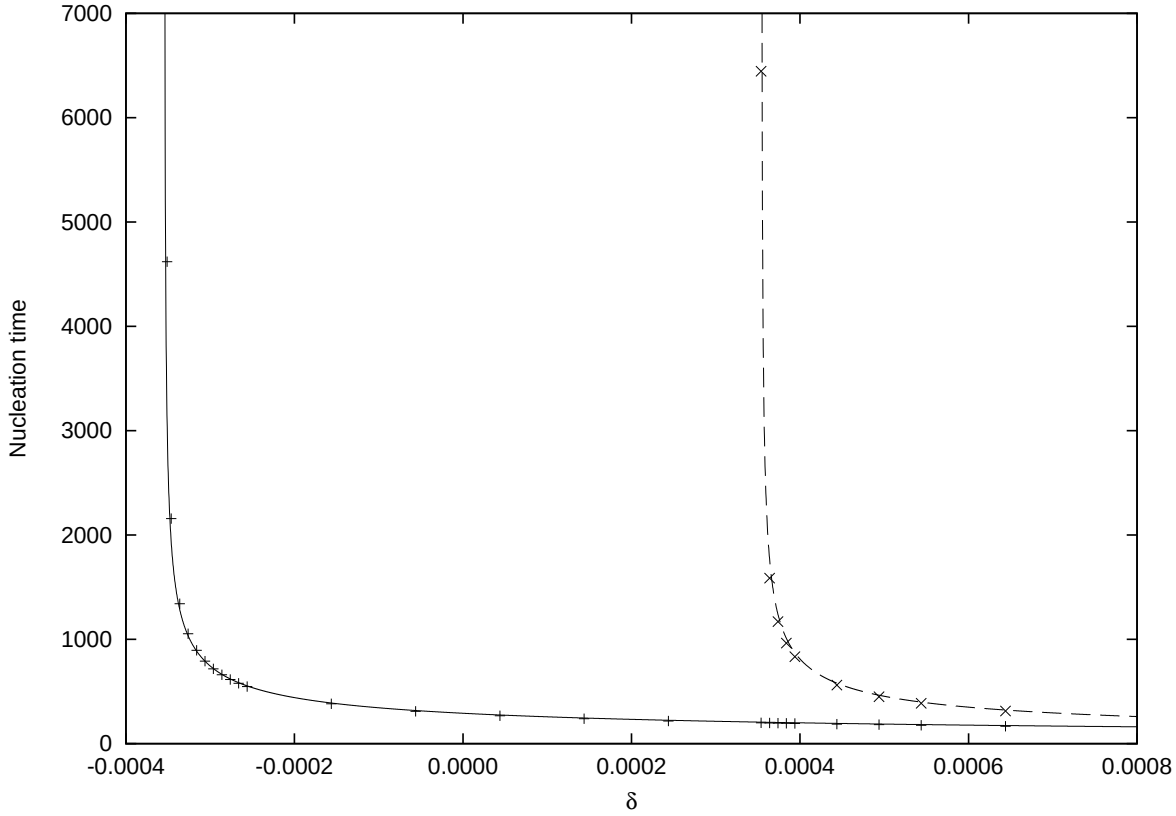

FIG. 9: Predicted leading (left curve) and trailing (right curve) nucleation times as a function of $\delta \equiv r - r_{P2}$ when $\gamma = 0.001$. When $\delta = 0.00015$ growth takes place at the leading front only (Fig. 7a); when $\delta = 0.00065$ it takes place at both front and back (Fig. 7b). The analytical predictions (continuous lines) are in excellent agreement with direct numerical simulation (superposed data points).

examined the effects of dispersion on the motion of fronts just outside the pinning region, and showed by means of numerical simulations and analysis that for small dispersion nucleation occurs at the leading front but with increasing distance from the upper boundary of the pinning region two-sided nucleation takes over. Our analytical prediction of this transition matches almost perfectly the numerical results. Analogous results are obtained near the lower boundary of the pinning region, although here the localized structure is gradually eroded as the domain fills with the trivial state.

As shown in Fig. 7(c) increasing the dispersion for fixed distance from the pinning region arrests the growth at the trailing front and restores one-sided nucleation. This transition is a manifestation of the transition from nonlinear absolute instability to nonlinear convective

instability [12] and so is distinct from the transition studied in this article.

Acknowledgments

This research was supported by NSF grant DMS-0605238 (JB and EK) and by EPSRC grant EP/D032334/1 (SMH).

---

[1] J. Burke and E. Knobloch, Phys. Rev. E **73**, 056211 (2006).

[2] J. Burke and E. Knobloch, Chaos **17**, 037102 (2007).

[3] C. J. Budd and R. Kuske, Physica D **208**, 73 (2005).

[4] Y. Pomeau, Physica D **23**, 3 (1986).

[5] S. J. Chapman and G. Kozyreff, Physica D **238**, 319 (2009).

[6] P. D. Woods and A. R. Champneys, Physica D **129**, 147 (1999).

[7] P. Coullet, C. Riera, and C. Tresser, Phys. Rev. Lett. **84**, 3069 (2000).

[8] M. Beck, J. Knobloch, D. J. B. Lloyd, B. Sandstede, and T. Wagenknecht, SIAM J. Math. Anal. **41**, 936 (2009).

[9] I. S. Aranson, B. A. Malomed, L. M. Pismen, and L. S. Tsimring, Phys. Rev. E **62:R5**, R5 (2000).

[10] J. Burke and E. Knobloch, Proc. 7th AIMS Conference, Arlington, TX, in press (2009).

[11] M. K. Wadee, C. D. Coman, and A. P. Bassom, Physica D **163**, 26 (2002).

[12] J.-M. Chomaz, Phys. Rev. Lett. **69**, 1931 (1992).